On DMT methods to calculate adhesion in rough contacts

G. Violano, L. Afferrante[1,*]

[1]*Department of Mechanics, Mathematics and Management, Politecnico of Bari, V.le Japigia, 182, 70126, Bari, Italy*

Abstract

In this paper, we compare different rough contact-mechanics theories with the assumption of weak interfacial adhesion. Two different approaches for the local modeling of adhesion are also considered: the DMT force approach (DMT-F) and the Maugis' approximation (DMT-M). The first approach is based on the idea of summing up attractive interactions that act outside the contact zone; the latter considers a constant adhesive load for each asperity in contact.

A comparison with numerical data proves the DMT-F approach is very accurate when hard solids and low adhesive interactions are considered. The DMT-M approach shows, instead, less accuracy especially at low fractal dimensions.

Keywords: Adhesion; rough contact mechanics; pull-off force; DMT theory

*Corresponding author. Email:luciano.afferrante@poliba.it,phonenumber:+390805962704

I. INTRODUCTION

One of the main recent challenges in the rough contact mechanics is the evaluation of the pull-off force necessary to detach sticky surfaces. The pull-off force plays a crucial role in various fields such as medicine, engineering, and biology. For example, to study processes of pulmonary drug delivery for asthma treatment, Beach et al. [1] measured the pull-off force between pharmaceutical particles and rough polymeric surfaces. They found the surface roughness strongly influences the pull-off force. Ramakrishna et al. [2] obtained similar results studying adhesion and friction properties of the elastic contact between a sphere and nanoparticle gradient surfaces. They performed pull-off force measurements at various levels of particle density. At high particle density, the short ranged adhesion mechanism is preponderant. Decreasing particle density, long ranged non-contact interactions become dominant. The first case falls under the Johnson, Kendall & Roberts (JKR) theory [3], which well describes the contact of soft materials with high values of surface energy. In the latter case, we are in the framework of the Derjaguin, Muller & Toporov (DMT) theory [4], which well captures the adhesion behavior of hard elastic materials with small values of surface energy.

In the design of biomimetic adhesive surfaces, controlling the detachment force is of crucial importance [5]. Biomimetic surfaces often show strong adhesive properties and are not adequate for locomotion devices. Recent studies analyzed the influence of the surface topography on detachment mechanisms [6, 7]. In particular, in the case of complex rough geometries, surface anisotropy can be exploited in the design of direction-dependent adhesives [8]. Dening et al. [9] studied the contact between a spherical indenter and an inflatable membrane, showing that the pull-off force reduces by decreasing the radius of curvature of the membrane.

In particular, with reference to a rigid sphere of radius R squeezed over an elastic half-space, the pull-off force predicted by the JKR and DMT theories is, respectively, $1.5\pi\Delta\gamma R$ and $2\pi\Delta\gamma R$, being $\Delta\gamma$ the surface energy of the two bodies in contact. The Tabor parameter μ [10] governs the transition from the JKR to DMT limit. Many authors give different, although similar, definitions of the Tabor parameter. In this work, we use the definition proposed by Greenwood in Ref. [11], according to which $\mu = (R\Delta\gamma^2/E^{*^2})^{1/3}/\varepsilon$, where E^* is the composite elastic modulus and ε is the range of action of adhesive forces.

Numerous theories and models have been formulated over the past years to investigate the effect of roughness on adhesion. A Boundary Element Method (BEM) based on the use of proper Green's functions has been developed in Refs. [12, 13] for 1D one-length scale rough profiles, and in Ref. [14] for 1D self-affine fractal profiles. A multiscale approach has been instead proposed in Ref. [15] to describe the elastic contact between 1D rough profiles. Here the solution for partial contact of a sinusoidal profile is used to develop a relationship between the pressures at different magnifications; then the contact area is calculated in terms of the magnification with a recursive formula.

Muser, instead, developed a Green's Function Molecular Dynamics (GFMD) method to study the contact mechanics of 2D randomly rough surfaces [16, 17], using a Fourier spacing formulation. Persson proposed a very robust analytical theory [18, 19], which has been also extended to the adhesive case [20, 21]. Medina & Dini [22] presented a model based on a Multi-Level Multi-Integration technique that solves adhesive rough contact by integrating the Lennard-Jones potential. Pastewka & Robbins (PR) [23] developed a theory to capture the interplay between elasticity, interatomic attraction, and surface roughness. Also, they formulated a criterion for sticky adhesion. Rey et al. [24] implemented an algorithm based on the Fast Fourier Transform (FFT) to compute the solution of adhesive normal contact between rough surfaces.

Many of the aforementioned models, although very accurate in returning the contact problem solution, require heavy computational costs.

Inspired from the excellent results obtained in the recent Contact Mechanics Challenge with the Interacting and Coalescing Hertzian Asperity model, we extend such model to the adhesive case in the limit of hard solids and small values of surface adhesion energy. Therefore, adhesive stresses can be assumed not involving deformations, according to the DMT theory. Adhesion is introduced in the model in two ways: (i) by integrating an interaction potential law above the non-contact area (DMT force approach, DMT-F), and (ii) using the Maugis' idea [26] which assumes constant adhesive load on each asperity in contact (DMT-M). In the latter case, the total adhesive force is then obtained by summing all asperities contributions. A comparison with numerical data available in the literature and Persson's theoretical predictions shows the DMT-F approach leads to good results, while non-negligible qualitative and quantitative discrepancies are found with the DMT-M method.

II. METHODS

Consider a linear elastic half-space, with Young's modulus E and Poisson's ratio ν, squeezed against a hard randomly rough substrate. Roughness is described by a self-affine fractal geometry, i.e. the surface does not change its morphology if we make a scale change. For an isotropic self-affine surface the power spectral density (PSD) has a power law relation with the magnitude $q = |\mathbf{q}|$ of the wave vector $\mathbf{q}$. Moreover, since many real surfaces have a long distance roll-off wavelength λ_0 corresponding to a wavevector $q_0 = 2\pi/\lambda_0$, in this work we consider isotropic self-affine fractal surfaces with PSD

$$C(\mathbf{q}) = \begin{cases} C_0 & \text{if } q_L \leq q \leq q_0 \\ C_0 q^{-2(H+1)} & \text{if } q_0 \leq q \leq q_1 \end{cases} \tag{1}$$

and zero otherwise. The parameter H is the Hurst exponent, which is related to the fractal dimension $D_f = 3 - H$. Further, we have indicated with $q_L = 2\pi/L$ the smallest possible wave vector which depends on the lateral size L of the surface region and with $q_1 = Nq_0$ the high-frequency cut-off, where N is the number of scales. Rough surfaces are numerically generated according to the spectral method developed in Ref. [28].

A. Interacting and Coalescing Hertzian Asperities (ICHA) model

In Ref. [29], an advanced multiasperity model is developed to study the contact mechanics of rough surfaces. The model is based on the original idea of GW theory [30] to replace the surface summits with spherical asperities with the same radius. However, numerous improvements are implemented. First, summits are replaced with spheres with radius equal to the geometric mean of the two principal radii of curvature. Indeed, Greenwood [31] showed that, in this way, almost the same results are obtained as in the Bush, Gibson, and Thomas (BGT) theory [32], who modeled the asperities as paraboloids with two different radii of curvature.

Furthermore, the elastic coupling between asperities is taken into account according to Ref. [33], where the asperity displacement is calculated using the Hertz theory and even considering the effect of the other asperities, which is added to the self-displacement. For a single rigid axisymmetric parabolic asperity approaching the elastic half-space, the standard

Hertzian formulas for the surface displacements can be found in Ref. [34]

$$u(r) = \frac{1}{R}\left(a^2 - \frac{r^2}{2}\right), \qquad r \leq a$$
$$u(r) = \frac{1}{\pi R}\left[\left(2a^2 - r\right)\arcsin\frac{a}{r} + a\sqrt{r^2 - a^2}\right], \qquad r > a$$

where a is the radius of the contact spot and R is the geometric mean of the principal radii of curvature.

For a given distribution of contact radii a_i, the displacement of the elastic half-space at the kth asperity is then obtained by summing the contribution of all asperities in contact.

The coalescence of contact spots is also taken into account. In fact, when two contact spots of adjacent asperities grow up to overlap, a single contact patch is formed. In Ref. [35] the coalescence of crystallite grains is studied and the mutual adhesion stresses are calculated. Freund & Chason [36] proposed a theoretical approach to calculate stresses generated upon contact of neighboring patches. However, the complexity of rough surfaces requires to look for empirical solutions. Specifically, in Ref. [29] merging asperities are replaced with a new equivalent one, which preserves the total contact area of the coalescing spots and their volume centroid. The radius of curvature of the new asperity R_{eqv} is instead assumed equal to $\left(R_i^2 + R_j^2\right)^{1/2}$, being R_i and R_j the radii of curvature of the merging asperities.

Finally, the local gap outside the contact spots in a generic point P is obtained by summing the contribution due to each asperity, as explained in Ref. [37], i.e.

$$u(P) = \frac{1}{\pi}\sum_{k=1}^{n_c}\left(\frac{2a_k^2 - r_{Pk}^2}{R_k}\arcsin\frac{a_k}{r_{Pk}} + \frac{a_k}{R_k}\sqrt{r_{Pk}^2 - a_k^2}\right) \tag{2}$$

being r_{Pk} the distance of the point P from the kth asperity and n_c the total number of asperities in contact.

In the limit of hard elastic solids with long ranged adhesive interactions (i.e. small values of the Tabor parameter μ), adhesion can be described by the DMT theory, which assumes no adhesive stresses act within the contact area. Adhesion interactions are concentrated outside the contact area, and deformation is exclusively due to the mechanical compressive component of the load.

More than one version of the DMT theory exists in the literature. In particular, Muller et al. [38] solved the adhesive elastic contact between spheres with two different approaches. The first one (known as DMT thermodynamic approach) is based on the calculation of the derivative of the adhesive interaction energy. The second approach (DMT force approach), instead, returns adhesive load by summing the attractive interactions acting between bodies. As shown by Pashley [39] and later by Greenwood [11], in the case of adhesive spherical contact, the DMT force approach correctly estimates the pull-off force value when $\mu < 0.24$.

In this work, according to the procedure developed in Ref. [21], the force approach is extended to complex rough geometries. To this end, a gap dependent adhesive force per unit area $\sigma_a(u)$ is introduced

$$\sigma_a(u) = \frac{8}{3}\frac{\Delta\gamma}{\varepsilon}\left[\left(\frac{\varepsilon}{u+\varepsilon}\right)^3 - \left(\frac{\varepsilon}{u+\varepsilon}\right)^9\right] \tag{3}$$

where ε is the range of action of attractive forces, which is of the order of magnitude of the atomic spacing. Therefore, the adhesive load F_{ad} is calculated as

$$F_{ad} = \int_{A_{nc}} d^2x \sigma_a\left[u\left(\mathbf{x}\right)\right] \tag{4}$$

where A_{nc} is the non-contact area. Moreover, if $P(u)$ denotes the probability gap distribution, then (4) can be written as

$$F_{ad} = A_0 \int_0^\infty \sigma_a(u) P(u) du \tag{5}$$

being A_0 the nominal contact area.

In the DMT limit, adhesive interactions don not affect deformations; however, it is assumed that deformations are due to an effective load F_0, which contains the external applied load F_N and the contribution from the adhesive force F_{ad}, $F_0 = F_N + F_{ad}$.

Maugis, in Ref. [26], proposed a different, but very simple approach, to extend the GW theory to the adhesive problem. For each asperity, the adhesive load is assumed to be constant and equal to the value of the tensile force which appears at the pull-off of a sphere with the same radius R of the asperity. As a result, the adhesive term can be calculated by assigning to each asperity in contact an adhesive load equal to $2\pi\Delta\gamma R$. Therefore, when

asperities with different radii of curvature R_i are considered, the adhesive load would write as

$$F_{ad} = \sum_{i=1}^{n_c} 2\pi\Delta\gamma R_i \tag{6}$$

B. Persson's theory: a brief outline

In the framework of Persson's theory [40], the relative contact area is

$$\frac{A}{A_0} = \mathrm{erf}\left(\frac{F_N}{A_0\sqrt{\langle\nabla h^2\rangle/2}E^*}\right) \tag{7}$$

where $\langle\nabla h^2\rangle = \int_{q_L}^{q_1} d^2q\, q^2 C(\mathbf{q})$ is the averaged square slope of the surface heights. Eq. (7) returns the correct solution close to complete contact, but, as we move towards small loads, the estimation of the contact area becomes less accurate. A better estimation of the contact area (see Ref. [41]) can be obtained by replacing $\langle\nabla h^2\rangle$ with $\langle\nabla u^2\rangle = \int_{q_L}^{q_1} d^2q\, q^2 C(\mathbf{q})\, S(q)$, which can be interpreted as the averaged square slope of the deformed surface. Therefore, the original assumption to consider the PSD of the deformed profile in partial contact equal to that in full contact is corrected by scaling $C(\mathbf{q})$ with the quantity $S(q) = \gamma + (1-\gamma)\left[A(q)/A_0\right]^2$. The parameter γ is a universal constant which can be approximately assumed equal to 0.45.

As above mentioned, in Ref. [21] solution of the adhesive problem is obtained by substituting F_N with the effective load F_0 in the area vs. load relation (7). Moreover, the adhesive force F_{ad} is calculated according to (5), where the gap probability distribution, originally derived in Ref. [42], is calculated in terms of the separation u and magnification $\zeta = q_1/q_L$

$$\begin{aligned} P(u) \;\approx\; & \frac{1}{A_0}\int d\zeta \frac{-A'(\zeta)}{(2\pi h^2_{\mathrm{rms}}(\zeta))^{1/2}} \times \\ & \left[\exp\left(-\frac{(u-u_1(\zeta))^2}{2h^2_{\mathrm{rms}}(\zeta)}\right) + \exp\left(-\frac{(u+u_1(\zeta))^2}{2h^2_{\mathrm{rms}}(\zeta)}\right)\right] \end{aligned} \tag{8}$$

where $u_1(\zeta)$ is the (average) separation in the surface area which (appears) to move out of contact as the magnification increases from ζ to $\zeta + d\zeta$ and is predicted by the Persson theory according to [43]

$$u_1(\zeta) = \bar{u}(\zeta) + \bar{u}'(\zeta)\, A(\zeta)/A'(\zeta) \tag{9}$$

where the apex symbol denotes the derivative with respect to the magnification ζ.

The quantity $h^2_{\rm rms}(\zeta)$ is the mean of the square of the surface roughness amplitude including only roughness components with the wavevector $q > q_0\zeta$, i.e.

$$h^2_{\rm rms}(\zeta) = \int_{q>q_0\zeta} d^2q\ C(\mathbf{q}). \tag{10}$$

Recently, in Ref. [37], a slightly more accurate expression for $P(u)$ is introduced, in which the term $h_{\rm rms}(\zeta)$ is replaced with

$$h^{\rm eff}_{\rm rms}(\zeta) = \left[h^{-2}_{\rm rms}(\zeta) + u_1^{-2}(\zeta)\right]^{-1/2}. \tag{11}$$

The new expression takes into account that fluctuations in the separation, occurring in the surface area $dA(\zeta)$ which moves out of contact as the magnification increases from ζ to $\zeta + d\zeta$, can be larger than $u_1(\zeta)$.

In this work, Persson's results are presented by considering both the corrections given in Refs. [37, 41] about the contact area and probability distribution of interfacial separations.

III. RESULTS

This section is divided into two parts. In the first one, the advanced version of the Persson's theory and ICHA model are compared with numerical data available in the literature.

The Maugis' approximation is very often quoted in the literature as the actual DMT's contribution (see Ref. [11]). Moreover, the extension of the original GW theory to the adhesive case is frequently developed in the framework of the Maugis' approximation (Refs. [26, 27]). For this reason, in the second part of this section, a comparison between the Maugis' approach [26] and DMT force method [38] is proposed in the framework of the ICHA model.

A. Persson's theory and ICHA model

Figs. 1-3 show a comparison between the advanced Persson's theory and ICHA model with the exact numerical simulations given in Persson & Scaraggi (PS) [21].

In particular, we refer to the PS data obtained on self-affine fractal surfaces with Hurst exponent $H = 0.8$, cut-off spatial frequency $q_L = 2.5\times10^5$ m^{-1}, and roll-off spatial frequency

$q_0 = 4q_L$. The PSD was truncated at $q_1 = 64q_L$, resulting in a root mean square roughness $h_{rms} = 0.52$ nm and root mean square slope $h'_{rms} = 0.00115$. Moreover, simulations were carried out for $E^* = 1.33 \times 10^3$ GPa and different values of the adhesion surface energy $\Delta\gamma = 0.1, 0.2, 0.3, 0.4$ J/m^2 (corresponding to a Tabor parameter μ ranging from 0.114 to 0.287).

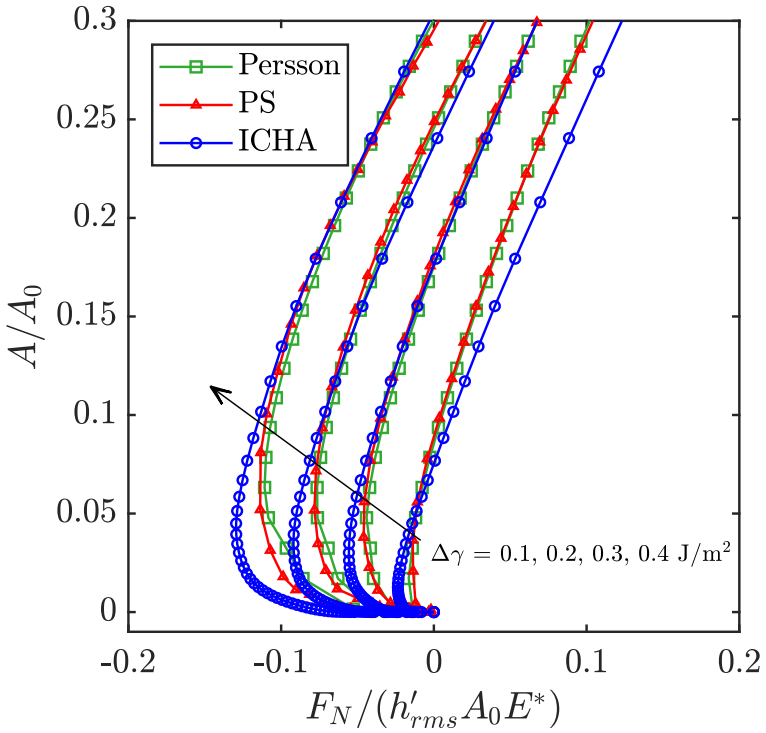

FIG. 1: The relative contact area A/A_0 as a function of the dimensionless applied pressure $F_N/(E^*A_0h'_{\rm rms})$ for different values of the surface energy of adhesion $\Delta\gamma$. Results are obtained on a self-affine surface with $H = 0.8$, $q_L = 2.5 \times 10^5$ m^{-1}, and $q_0 = 4q_L$. The PSD was truncated at $q_1 = 64q_L$, resulting in a root mean square roughness $h_{rms} = 0.52$ nm and root mean square slope $h'_{rms} = 0.00115$.

Fig. 1 shows the relative contact area A/A_0 as a function of the dimensionless applied pressure $F_N/(E^*A_0h'_{\rm rms})$ for different values of the surface energy of adhesion $\Delta\gamma$. The agreement with numerical simulations (red lines with triangular markers) is very satisfactory. However, at the higher values of $\Delta\gamma$ the ICHA model (blue line with circular markers) seems slightly overestimating the adhesive force at the smaller values of the contact area. The advanced version of the Persson's theory (green line with square markers) is instead always in perfect agreement with numerical data.

In the DMT limit, adhesive hysteresis is neglected, then no differences occur between loading and unloading curves. Under such a hypothesis, the pull-off force is equal to the

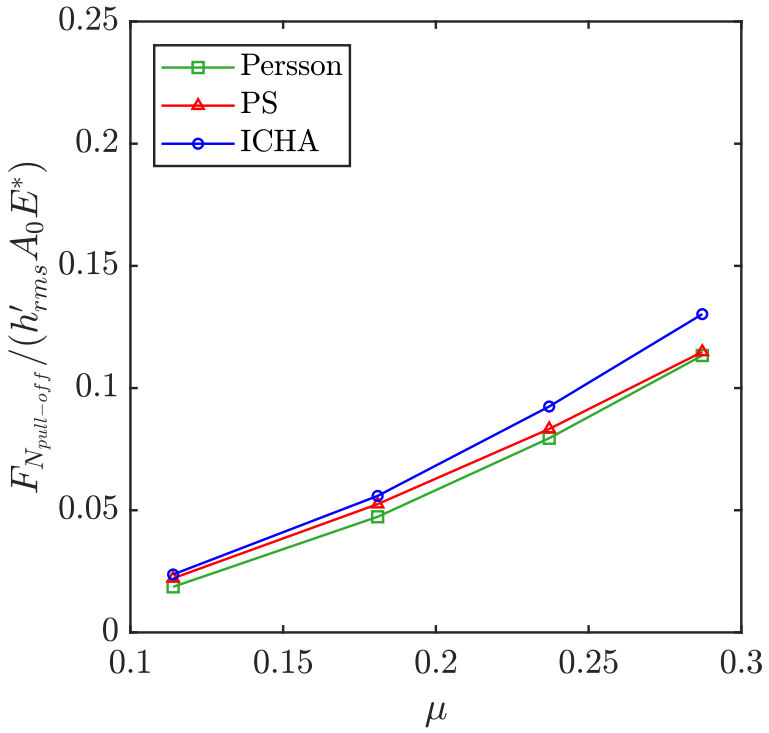

FIG. 2: The dimensionless pull-off force $F_{N_{pull-off}}/(E^*A_0h'_{\rm rms})$ as a function of the Tabor parameter μ. Results are obtained on a self-affine surface with $H = 0.8$, $q_L = 2.5 \times 10^5$ m^{-1}, and $q_0 = 4q_L$. The PSD was truncated at $q_1 = 64q_L$, resulting in a root mean square roughness $h_{rms} = 0.52$ nm and root mean square slope $h'_{rms} = 0.00115$.

magnitude of the largest tensile load. The influence of the Tabor parameter on the pull-off force is shown in Fig. 2. As expected, the pull-off force increases with μ. The theoretical models well agree with the numerical data again.

Fig. 3 shows the normalized mean interfacial separation $\bar{u}/h_{rms}$ as a function of the applied force. Both Persson's theory and ICHA model closely match numerical data with some small discrepancy in the range of low gaps at the higher values of $\Delta\gamma$ (in particular as far as the Persson's predictions are concerned).

The above results suggest adhesive models based on the DMT theory rightly predict the main contact quantities of rough contacts in the range of $\mu < 0.3$.

A comparison with the numerical simulations of Pastewka&Robbins (PR) [23] is also proposed to investigate the contact behavior for higher values of the Tabor parameter. This choice is related to the observation that in the numerical cases investigated in Ref. [23] adhesion produces a small change in surface deformation, indicating that we are still close to the DMT limit.

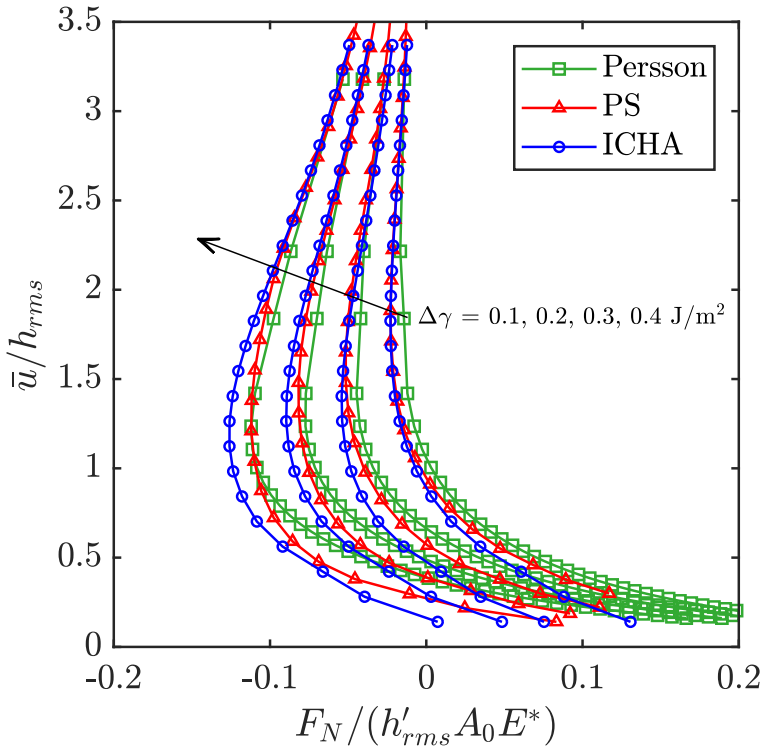

FIG. 3: The dimensionless mean interfacial separation $\bar{u}/h_{\rm rms}$ as a function of the dimensionless applied pressure $F_N/(E^*A_0h'_{\rm rms})$ for different values of the surface energy of adhesion $\Delta\gamma$. Results are obtained on a self-affine surface with $H = 0.8$, $q_L = 2.5 \times 10^5$ m^{-1}, and $q_0 = 4q_L$. The PSD was truncated at $q_1 = 64q_L$, resulting in a root mean square roughness $h_{rms} = 0.52$ nm and root mean square slope $h'_{rms} = 0.00115$.

Specifically, we refer to PR calculations performed on self-affine surfaces with $H = 0.3$, 0.5, 0.8 and number of scales $N = q_1/q_0 = 32, ...\ 256$. Moreover, data are obtained for $E^* = 10^3$ GPa and $\Delta\gamma = 5$, 10 J/m^2 (corresponding to values of the Tabor parameter $\mu = 0.552$ and $\mu = 0.876$, respectively). However, PR used a small amount of roll-off ($q_0 = 2q_L$), and this entails scatter in results and finite size effects. For this reason, the ICHA predictions were averaged on results obtained from 10 different realizations of the surface. For all surfaces, roughness was generated by keeping constant the root mean square slope $h'_{\rm rms} = 0.1$.

In Fig. 4 the relative contact area A/A_0 is plotted in terms of the contact pressure $F_N/(E^*A_0h'_{\rm rms})$ for $\mu = 0.552$ (Fig. 4a) and $\mu = 0.876$ (Fig. 4b). Results are shown for a surface with $H = 0.8$ and $N = 64$.

At $\mu = 0.552$, the ICHA model (blue line with circular markers) and Persson's theory predictions (green line with square markers) are very close to PR data (red line with tri-

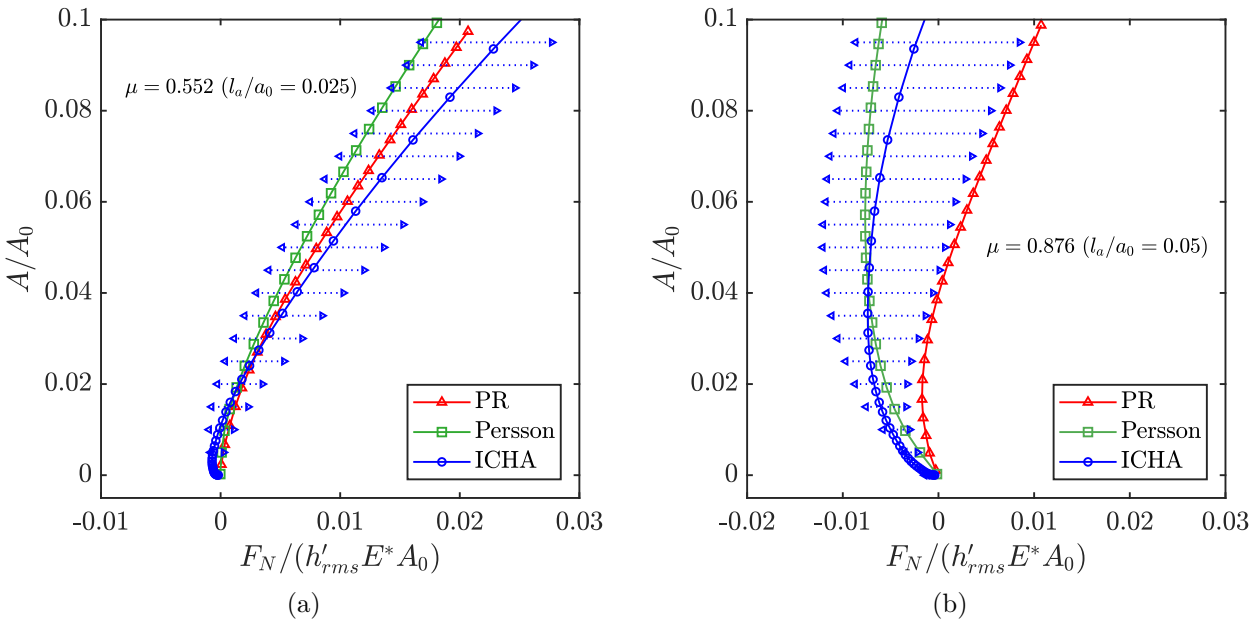

FIG. 4: The relative contact area A/A_0 as a function of the dimensionless applied pressure $F_N/(E^*A_0h'_{\rm rms})$ for $\mu = 0.552$ ($l_a/a_0 = \Delta\gamma/\left(E^*a_0\right) = 0.025$) (Fig. 4a) and $\mu = 0.876$ ($l_a/a_0 = 0.05$) (Fig. 4b). Error bars (dotted arrows) show scatter of results of the ICHA model as they are averaged on 10 different surface realizations. Calculations are performed on self-affine fractal surfaces with $N = 64$, $H = 0.8$, and $h'_{\rm rms} = 0.1$.

angular markers). Error bars (dotted arrows), relative to the ICHA results, make clear the existence of a non-negligible scatter in results due to the very little roll-off used ($q_0/q_L = 2$) to generate the surfaces.

At $\mu = 0.876$, both Persson theory and ICHA model return larger adhesive effects than PR numerical results. Such discrepancy can be justified by observing that PR data are obtained on a single realization of the self-affine surface, which can significantly deviate from a Gaussian one [44] because of the very little roll-off used in generating the surface. Persson's and ICHA model predictions instead refer to average results. Secondly, increasing the Tabor parameter, adhesion involves bodies deformation, and thus we are no longer in a strict DMT limit. Finally, we notice PR use a different relationship for the attractive force. In particular, attractive interactions are described by a spline potential law which considers a repulsive contribution for separations smaller than the atomic spacing a_0. On the contrary, the potential law returning the adhesive force per unit area of Eq. (3) neglects repulsive interactions.

Fig. 5 shows the normalized pull-off force as a function of N for three different values

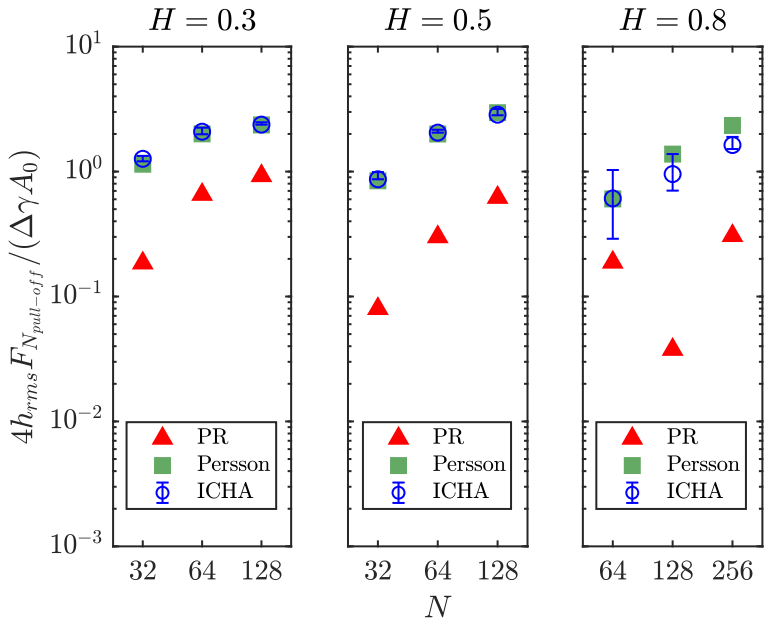

FIG. 5: The normalized pull-off force for different values of the number of scales N and Hurst exponent ($H = 0.3, 0.5, 0.8$). Calculations are performed for $\mu = 0.876$ ($l_a/a_0 = 0.05$) and on surfaces with $h'_{\rm rms} = 0.1$. Error bars refer to the minimum and maximum pull-off force obtained with ICHA model, as they are averaged on 10 different surface realizations.

of H. The force normalization is the same as proposed by PR in Ref. [23]. Red triangles refer to PR data, while green squares and blue circles refer to Persson's theory and ICHA model, respectively. Error bars denote the minimum and maximum values of the pull-off force predicted by the ICHA model. Scatter is much more relevant for surfaces with few asperities (i.e., with high H and low N). ICHA predictions are very close to the Persson ones but are higher than PR data. Such difference can be explained by observing that at $\mu = 0.876$ adhesive interactions are sufficiently large to deform the half-space, then the validity of the DMT approximation becomes questionable. Nevertheless, the trend with H and N is very similar to PR data (except the outlier observed at $H = 0.8$ and $N = 128$, which can be partly explained in terms of the scatter of results as PR performed calculations only on a single surface realization).

Finally, in Fig. 6, we observe the pull-off force decays with the rms roughness amplitude $h_{\rm rms}$.

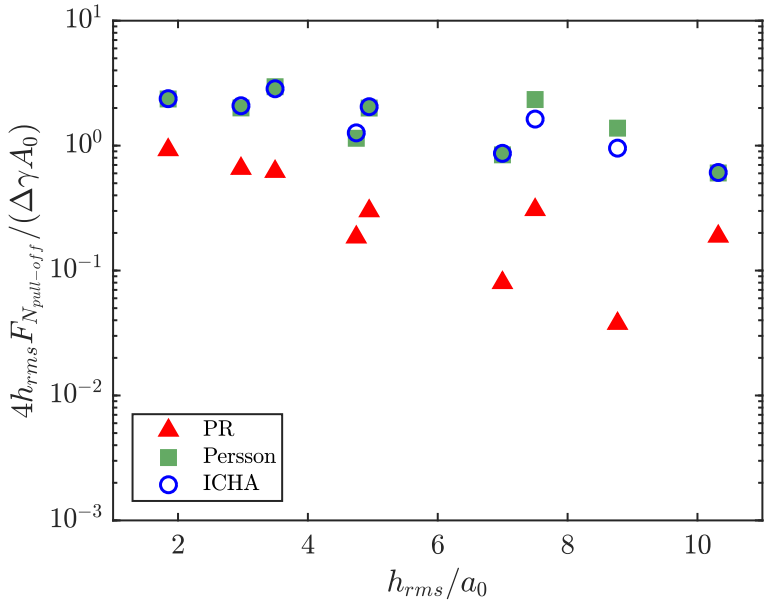

FIG. 6: The normalized pull-off force as a function of the dimensionless rms roughness amplitude $h_{\rm rms}/a_0$. Calculations are performed for $\mu = 0.876$ ($l_a/a_0 = 0.05$) and on surfaces with $h'_{\rm rms} = 0.1$.

B. On DMT methods to calculate adhesive interactions

In this section, results obtained implementing the DMT force approach (DMT-F) in the ICHA model are compared with a different method to include adhesion, based on the Maugis' idea (DMT-M) [26].

Calculations are performed on a squared area with lateral size $L = 2\pi/(2.5 \cdot 10^5)$ m and self-affine fractal surfaces characterized by $h_{\rm rms} = 0.52$ nm and wavevector frequencies $q_L = 2\pi/L$, $q_0 = 4q_L$, and $q_1 = Nq_0$. Moreover, we have assumed $\Delta\gamma = 0.2$ J/m^2 and $E^* = 1.33 \times 10^3$ GPa.

Fig. 7 shows the relative contact area A/A_0 as a function of the dimensionless applied pressure $F_N/(E^* A_0 h'_{\rm rms})$ for $N = 64$ and $H = 0.8$. Results are presented for both the DMT-F (blue circles), and DMT-M (red triangles) approaches. Persson's predictions (green squares) are also plotted for comparison.

The Maugis approach leads to very different results in terms of area-load relation, while a very good agreement is observed between Persson's theory and ICHA model based on DMT-F approach.

The same type of comparison is proposed in Fig. 8 in terms of the dimensionless interfacial

mean separation $\bar{u}/h_{\mathrm{rms}}$. Once again the DMT-M results significantly deviate from the predictions of Persson's theory, which instead are in close agreement with the DMT-F ones.

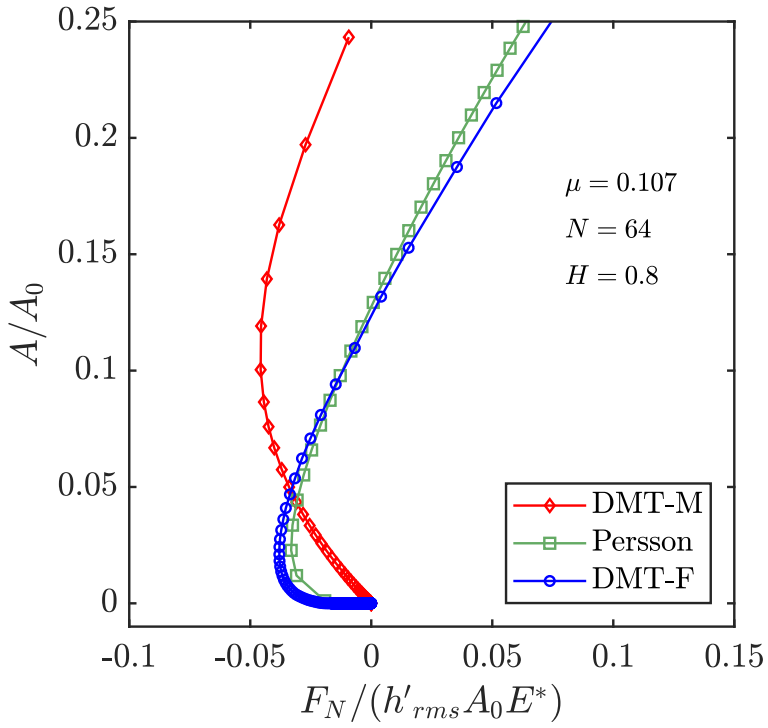

FIG. 7: The relative contact area A/A_0 as a function of the dimensionless applied load $F_N/(E^*A_0h'_{\mathrm{rms}})$. Calculations are performed for $\Delta\gamma = 0.2$ J/m^2, $E^* = 1.33 \times 10^3$ GPa and on a surface with $N = 64$, $H = 0.8$ and $h_{\mathrm{rms}} = 0.52$ nm, resulting in a Tabor parameter $\mu = 0.107$. Persson's predictions are also plotted for comparison.

Fig. 9 shows the normalized pull-off force $F_{N_{pull-off}}/(A_0E^*)$ as a function of the modified Fuller & Tabor adhesion parameter $\theta_{FT} = E^*h_{\mathrm{rms}}^{3/2}R^{1/2}/(\Delta\gamma R)$ [45], which can be interpreted as the ratio between the elastic (repulsive) and adhesive contributions to the total load. Increasing θ_{FT}, a decay of the pull-off force is expected as the adhesion term reduces with respect to the elastic one. Results obtained with the DMT-F approach are consistent with this observation, while results based on the DMT-M approach give different trends depending on the value of the Hurst exponent H. In particular, we notice the pull-off force increases with θ_{FT} when $H > 0.5$.

Such apparent odd behavior can be explained by observing that the Maugis approximation gives an adhesive force contribution proportional to the product between the number of asperities in contact n_c and their mean radius of curvature $\bar{R}_c$. Therefore, in first approximation, we can consider the adhesive force dependent on the total number of surface

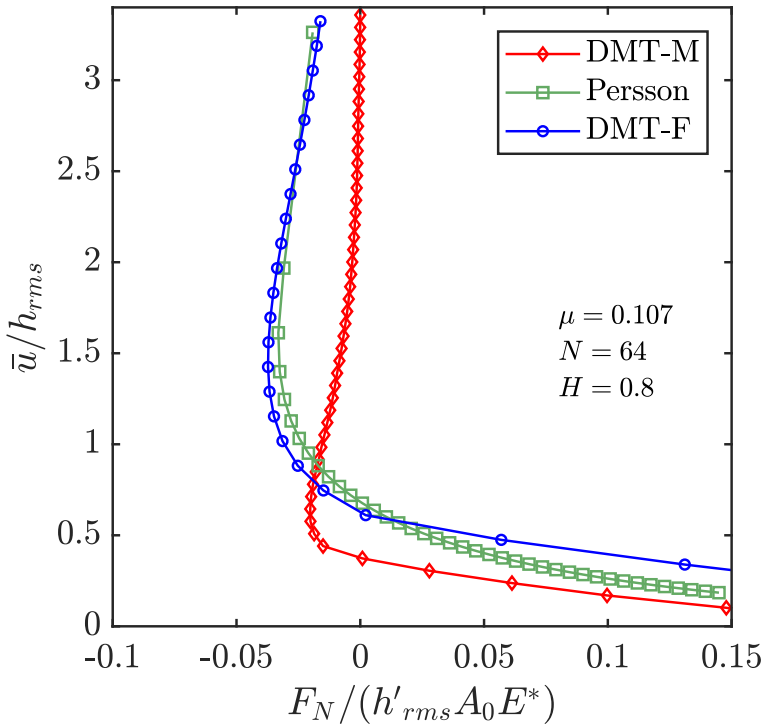

FIG. 8: The normalized mean interfacial separation $\bar{u}/h_{\rm rms}$ as a function of the dimensionless applied load $F_N/(E^*A_0h'_{\rm rms})$. Calculations are performed for $\Delta\gamma = 0.2$ J/m^2, $E^* = 1.33 \times 10^3$ GPa and on a surface with $N = 64$, $H = 0.8$ and $h_{\rm rms} = 0.52$ nm, resulting in a Tabor parameter $\mu = 0.107$. Persson's predictions are also plotted for comparison.

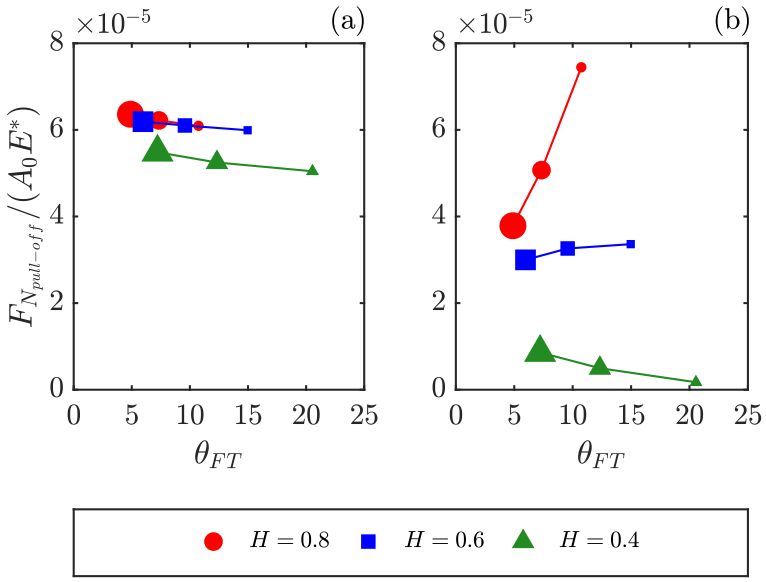

FIG. 9: The normalized pull-off force $F_{N_{pull-off}}/(A_0E^*)$ as a function of the adhesion parameter θ_{FT}. Results are given for different values of the Hurst exponent, $h_{\rm rms} = 0.52$ nm, and for both the DMT-F and DMT-M approaches. Symbols size decreases as N increases.

asperities n_{asp} and surface mean radius of curvature $\bar{R}$, related to the rms curvature $h''_{\rm rms}$ by $\bar{R} = 2/h''_{\rm rms}$. The total number of asperities, in turn, depends on the summits density d_{sum} in the nominal area A_0. According to Nayak's random process theory, we can estimate the density of summits as $d_{sum} \sim (h''_{\rm rms}/h'_{\rm rms})^2$. Therefore, taking into account that the mechanical repulsive contribution F_0 is proportional to the rms surface slope $h'_{\rm rms}$ [46–48], within the framework of Maugis approximation, we can write

$$\frac{F_0}{F_{ad}} \propto \frac{h'^3_{\rm rms}}{h''_{\rm rms}} \tag{12}$$

Now, observing that $h'_{\rm rms}$ and $h''_{\rm rms}$ are both functions of the scales number N and Hurst exponent H (or, equivalently, of the magnification $\zeta = q_1/q_L$ and H)

$$h'_{\rm rms} \sim \sqrt{\frac{\zeta^{2-2H}-1}{1-H}}; \qquad h''_{\rm rms} \sim \sqrt{\frac{\zeta^{4-2H}-1}{2-H}}, \tag{13}$$

Eq. (12) becomes

$$\frac{F_0}{F_{ad}} \propto \varphi(\zeta, H) = \frac{\zeta^{2-2H}-1}{1-H}\sqrt{\frac{2-H}{1-H}\frac{\zeta^{2-2H}-1}{\zeta^{4-2H}-1}} \tag{14}$$

At high fractal dimensions (namely $H < 0.5$), the function φ increases with the magnification ζ, that is the adhesive contribution reduces in comparison to the repulsive one. In such case, a decay of the pull-off force is expected according to the predictions given in Fig. 9b. This trend reverses at low fractal dimensions, then explaining the increase in pull-off force with θ_{FT} observed in Fig. 9b when $H > 0.5$ (being θ_{FT} an increasing function of ζ).

IV. CONCLUSIONS

In this paper, the adhesion between rough surfaces has been investigated with an advanced multiasperity contact model in the framework of the DMT theory. In particular, we have implemented adhesion according to (i) the DMT force approach (DMT-F), and the Maugis's approximation (DMT-F). The DMT-F approach assumes adhesive interactions act outside the contact area and do not deform the surface. The DMT-F approximation considers the adhesive load on each asperity to be constant and equal to the pull-off force of a sphere with

the same radius.

The DMT-F approach shows good qualitative agreement with numerical data provided by Persson & Scaraggi [21] and Pastewka & Robbins [23]. However, some discrepancy with PR data occurs for Tabor parameter close to 1. Such differences are partly due to the lack of statistic in PR results, which are calculated on a single realization of a surface with little roll-off. Moreover, increasing the Tabor parameter, the bodies deformation due to the adhesive interactions may not be neglected anymore, then we are no longer in a strict DMT limit.

About the DMT-M approach, results show non-negligible discrepancies with the reference data, especially at low fractal dimensions. Indeed, differently from what expected, a growth trend of the pull-off force with the modified Fuller & Tabor adhesion parameter θ_{FT} is observed when $H > 0.5$.

---

[1] Beach, E. R., Tormoen, G. W., Drelich, J., & Han, R. (2002). Pull-off force measurements between rough surfaces by atomic force microscopy. Journal of Colloid and Interface Science, 247(1), 84–99. https://doi.org/10.1006/jcis.2001.8126

[2] Ramakrishna, S. N., Nalam, P. C., Clasohm, L. Y., & Spencer, N. D. (2013). Study of adhesion and friction properties on a nanoparticle gradient surface: Transition from JKR to DMT contact mechanics. Langmuir, 29(1), 175–182. https://doi.org/10.1021/la304226v

[3] Johnson, K. L., Kendall, K., & Roberts, A. D. (1971). Surface Energy and the Contact of Elastic Solids. Proceedings of the Royal Society A: Mathematical, Physical and Engineering Sciences, 324(1558), 301–313. https://doi.org/10.1098/rspa.1971.0141

[4] Derjaguin, B. V., Muller, V. M., & Toporov, Y. P. (1975). Effect of contact deformations on the adhesion of particles. Journal of Colloid And Interface Science, 53(2), 314–326. https://doi.org/10.1016/0021-9797(75)90018-1

[5] Afferrante, L., & Carbone, G. (2012). Biomimetic surfaces with controlled direction-dependent adhesion. Journal of The Royal Society Interface, 9(77), 3359–3365. https://doi.org/10.1098/rsif.2012.0452

[6] Afferrante, L., Carbone, G., Demelio, G., & Pugno, N. (2013). Adhesion of elastic thin films: Double peeling of tapes versus axisymmetric peeling of membranes. Tribology Letters, 52(3),

439–447. https://doi.org/10.1007/s11249-013-0227-6

[7] Afferrante, L., & Carbone, G. (2013). The mechanisms of detachment of mushroom-shaped micro-pillars: From defect propagation to membrane peeling. Macromolecular Reaction Engineering, 7(11), 609–615. https://doi.org/10.1002/mren.201300125

[8] Afferrante, L., Grimaldi, G., Demelio, G., & Carbone, G. (2015). Direction-dependent adhesion of micro-walls based biomimetic adhesives. International Journal of Adhesion and Adhesives, 61, 93–98. https://doi.org/10.1016/j.ijadhadh.2015.05.007

[9] Dening, K., Heepe, L., Afferrante, L., Carbone, G., & Gorb, S. N. (2014). Adhesion control by inflation: implications from biology to artificial attachment device. Applied Physics A, 116(2), 567-573. https://doi.org/10.1007/s00339-014-8504-2

[10] Tabor, D. (1977). Surface forces and surface interactions. Journal of Colloid And Interface Science, 58(1), 2–13. https://doi.org/10.1016/0021-9797(77)90366-6

[11] Greenwood, J. A. (2007). On the DMT theory. Tribology Letters, 26(3), 203–211. https://doi.org/10.1007/s11249-006-9184-7

[12] Menga, N., Afferrante, L., Carbone, G. (2016). Adhesive and adhesiveless contact mechanics of elastic layers on slightly wavy rigid substrates. International Journal of Solids and Structures 88-89, 101-109.

[13] Carbone, G., & Mangialardi, L. (2008). Analysis of the adhesive contact of confined layers by using a Green's function approach. Journal of the Mechanics and Physics of Solids, 56(2), 684–706. https://doi.org/10.1016/j.jmps.2007.05.009

[14] Carbone, G., Scaraggi, M., & Tartaglino, U. (2009). Adhesive contact of rough surfaces: Comparison between numerical calculations and analytical theories. European Physical Journal E, 30(1), 65–74. https://doi.org/10.1140/epje/i2009-10508-5

[15] Afferrante, L., Ciavarella, M., & Demelio, G., (2015). Adhesive contact of the Weierstrass profile. Proceedings of the Royal Society A: Mathematical, Physical and Engineering Sciences.471 (2182), Art. no. 20150248. https://doi.org/10.1098/rspa.2015.0248.

[16] Campana, C., Muser, M.H. (2006). Practical Green's function approach to the simulation of elastic semi-infinite solids. Phys. Rev. B 74(7), 075420.

[17] Müser, M. H. (2016). A dimensionless measure for adhesion and effects of the range of adhesion in contacts of nominally flat surfaces. Tribology International, 100, 41–47. https://doi.org/10.1016/j.triboint.2015.11.010

[18] Persson, B. N. J., & Tosatti, E. (2001). The effect of surface roughness on the adhesion of elastic solids. The Journal of Chemical Physics, 115(12), 5597–5610. https://doi.org/10.1063/1.1398300

[19] Persson, B. N. J. (2006). Contact mechanics for randomly rough surfaces. Surface Science Reports, 61(4), 201–227. https://doi.org/10.1016/j.surfrep.2006.04.001

[20] Persson, B. N. J. (2002). Adhesion between an elastic body and a randomly rough hard surface. European Physical Journal E, 8(4), 385–401. https://doi.org/10.1140/epje/i2002-10025-1.

[21] Persson, B. N. J., & Scaraggi, M. (2014). Theory of adhesion: Role of surface roughness. Journal of Chemical Physics, 141(12). https://doi.org/10.1063/1.4895789

[22] Medina, S., & Dini, D. (2014). A numerical model for the deterministic analysis of adhesive rough contacts down to the nano-scale. International Journal of Solids and Structures, 51(14), 2620–2632. https://doi.org/10.1016/j.ijsolstr.2014.03.033

[23] Pastewka, L., & Robbins, M. O. (2014). Contact between rough surfaces and a criterion for macroscopic adhesion. Proceedings of the National Academy of Sciences, 111(9), 3298–3303. https://doi.org/10.1073/pnas.1320846111

[24] Rey, V., Anciaux, G., & Molinari, J. F. (2017). Normal adhesive contact on rough surfaces: efficient algorithm for FFT-based BEM resolution. Computational Mechanics, 60(1), 69–81. https://doi.org/10.1007/s00466-017-1392-5

[25] M. H. Muser, W. B. Dapp, R. Bugnicourt, P. Sainsot, N. Lesaffre, T. A. Lubrecht, B.N.J. Persson, K. Harris, A. Bennett, K. Schulze, S. Rohde, P. Ifju, W.G. Sawyer, T. Angelini, H.A. E.sfahani, M. Kadkhodaei, S. Akbarzadeh, J.-J., Wu, G. Vorlaufer, A. Vernes, S. Solhjoo, A.I. Vakis, R.L. Jackson, Y. Xu, J. Streator, A. Rostami, D. Dini, S. Medina, G. Carbone, F. Bottiglione, L. Afferrante, J. Monti, L. Pastewka, M.O. Robbins, and J.A. Greenwood, Meeting the contact-mechanics challenge. Trib. Letters, 65, 118 (2017).

[26] Maugis, D. (1996). On the contact and adhesion of rough surfaces. Journal of Adhesion Science and Technology, 10(2), 161–175. https://doi.org/10.1163/156856196X00832.

[27] Prokopovicha, P. and Perni, S. (2011). Comparison of JKR- and DMT-based multi-asperity adhesion model: Theory and experiment. Colloids and Surfaces A: Physicochem. Eng. Aspects 38, 95–101, https://doi.org/10.1016/j.colsurfa.2011.01.011.

[28] Putignano, C., Afferrante, L., Carbone, G., & Demelio, G. (2012). A new efficient numerical method for contact mechanics of rough surfaces. International Journal of Solids and Structures,

49(2), 338–343. https://doi.org/10.1016/j.ijsolstr.2011.10.009

[29] Afferrante, L., Carbone, G., & Demelio, G. (2012). Interacting and coalescing Hertzian asperities: A new multiasperity contact model. Wear, 278–279, 28–33. https://doi.org/10.1016/j.wear.2011.12.013

[30] Greenwood, J. A., & Williamson, J. B. P. (1966). Contact of Nominally Flat Surfaces. Proceedings of the Royal Society A: Mathematical, Physical and Engineering Sciences, 295(1442), 300–319. https://doi.org/10.1098/rspa.1966.0242

[31] Greenwood, J.A.: A simplified elliptic model of rough surface contact. Wear, 261, 191–200 (2006).

[32] Bush, A.W., Gibson, R.D., Thomas, T.R.: The elastic contact of a rough surface. Wear, 35, 87–111 (1975).

[33] Ciavarella, M., Delfine, V., Demelio, G.: A "re-vitalized" Greenwood and Williamson model of elastic contact between fractal surfaces. J. Mech. Phys. Solids, 54, 2569–2591 (2006).

[34] Johnson, K.L., Contact mehanics. Cambridge University Press, Cambridge, UK (1985).

[35] Suh, A. Y., Yu, N., Lee, K. M., Polycarpou, A. A., & Johnson, H. T. (2004). Crystallite coalescence during film growth based on improved contact mechanics adhesion models. Journal of Applied Physics, 96(3), 1348–1359. https://doi.org/10.1063/1.1766099

[36] Freund, L. B., & Chason, E. (2001). Model for stress generated upon contact of neighboring islands on the surface of a substrate. Journal of Applied Physics, 89(9), 4866–4873. https://doi.org/10.1063/1.1359437

[37] Afferrante, L., Bottiglione, F., Putignano, C., Persson, B.N.J., Carbone, G. (2018) Elastic contact mechanics of randomly rough surfaces: an assessment of advanced asperity models and Persson's theory. Tribology Letters

[38] Muller, V. M., Derjaguin, B. V., & Toporov, Y. P. (1983). On two methods of calculation of the force of sticking of an elastic sphere to a rigid plane. Colloids and Surfaces, 7(3), 251–259. https://doi.org/10.1016/0166-6622(83)80051-1

[39] Pashley, M. D. (1984). Further consideration of the DMT model for elastic contact. Colloids and Surfaces, 12(C), 69–77. https://doi.org/10.1016/0166-6622(84)80090-6

[40] Persson, B. N. J. (2001). Theory of rubber friction and contact mechanics. The Journal of Chemical Physics, 115(8), 3840–3861. https://doi.org/10.1063/1.1388626

[41] Persson, B. N. J. (2008). On the elastic energy and stress correlation in the contact between

elastic solids with randomly rough surfaces. Journal of Physics Condensed Matter, 20(31). https://doi.org/10.1088/0953-8984/20/31/312001

[42] A. Almqqvist, C. Campana, N. Prodanov, and B. N. J. Persson, J. Mech. Phys. Solids 59, 2355 (2011).

[43] Yang, C., & Persson, B. N. J. (2008). Contact mechanics: contact area and interfacial separation from small contact to full contact. Journal of Physics Condensed Matter, 20(21) https://doi.org/10.1088/0953-8984/20/21/215214

[44] Ciavarella, M., Papangelo, A., & Afferrante, L. (2017). Adhesion between self-affine rough surfaces: Possible large effects in small deviations from the nominally Gaussian case. Tribology International, 109, 435–440. https://doi.org/10.1016/j.triboint.2017.01.003

[45] Fuller, K. N. G., & Tabor, D. (1975). The Effect of Surface Roughness on the Adhesion of Elastic Solids. Proceedings of the Royal Society A: Mathematical, Physical and Engineering Sciences, 345(1642), 327–342. https://doi.org/10.1098/rspa.1975.0138

[46] Carbone, G., & Bottiglione, F. (2008). Asperity contact theories: Do they predict linearity between contact area and load? Journal of the Mechanics and Physics of Solids, 56(8), 2555–2572. https://doi.org/10.1016/j.jmps.2008.03.011

[47] Putignano, C., Afferrante, L., Carbone, G., & Demelio, G. (2012). The influence of the statistical properties of self-affine surfaces in elastic contacts: A numerical investigation. Journal of the Mechanics and Physics of Solids, 60(5), 973-982.

[48] Putignano, C., Afferrante, L., Carbone, G., & Demelio, G. (2013). A multiscale analysis of elastic contacts and percolation threshold for numerically generated and real rough surfaces. Tribology International, 64, 148-154.